The role of low-energy electrons in the high-energy radiolysis of condensed CF_3I

2010 J. Phys.: Condens. Matter 22 084006

(http://iopscience.iop.org/0953-8984/22/8/084006)

J. Phys.: Condens. Matter **22** (2010) 084006 (7pp) doi:10.1088/0953-8984/22/8/084006

The role of low-energy electrons in the high-energy radiolysis of condensed CF_3I

Mahesh Rajappan, Lin L Zhu, Jizhou Wang, Graeme Gardner, Kevin Bu, Huiliang Mai, Madeleine Laupheimer, Yomay Shyur, Nuriesya S Abu Bakar, Samantha K Skinner-Hall, Christina Kim, Jaclyn M Haskins and Christopher R Arumainayagam[1]

Department of Chemistry, Wellesley College, Wellesley, MA 02481, USA

E-mail: carumain@wellesley.edu

Received 1 September 2009, in final form 13 October 2009
Published 4 February 2010
Online at stacks.iop.org/JPhysCM/22/084006

Abstract

The dynamics of electron-induced reactions in condensed trifluoroiodomethane (CF_3I) were studied under ultrahigh vacuum conditions. Seven CF_3I radiolysis products (C_2F_6, C_2F_5I, C_2F_3I, CF_2I_2, $C_2F_4I_2$, CFI_3 and $C_2F_3I_3$) were identified using temperature-programmed desorption experiments conducted after irradiation with 4 eV electrons. Although C_2F_6 formation at energies above 4 eV is ascribed to electron-induced electronic excitation followed by prompt dissociation of the C–I bond to form $\cdot CF_3$ radicals that dimerize, the formation of the other six radiolysis products at low sub-ionization incident electron energies is attributed to dissociative electron attachment (DEA) because of the observed resonance peaks in the radiolysis product yields as functions of incident electron energy ($\sim$2 to $\sim$7 eV). All seven CF_3I electron-induced reaction products were also identified following irradiation with 500 eV electrons. While dissociative electron attachment and/or electron impact excitation may play an important role in the high-energy radiation-induced synthesis of the high-yield product C_2F_6, a dramatic enhancement of up to $\sim 2 \times 10^4$ in product yield per electron at 500 eV relative to that at 4 eV for some products suggests, however, that DEA is not the dominant mechanism for the high-energy radiation-induced synthesis of those products.

(Some figures in this article are in colour only in the electronic version)

1. Introduction

The interaction between high-energy radiation (e.g. γ-rays, x-rays, electrons and ion beams) and matter produces, within a few attoseconds, copious numbers ($\sim 4 \times 10^4$ electrons MeV^{-1} of energy deposited) of non-thermal secondary low-energy electrons [1]. Although other secondary products such as excited species and ions also cause some radiation damage, the inelastic collisions of these low-energy electrons with molecules and atoms produce distinct energetic species that serve as the primary driving forces in a wide variety of radiation-induced chemical reactions [2–4]. The energy distribution of the secondary electrons is such that the majority of these electrons typically have energies below 10 eV, as shown schematically in figure 1(a). The prominent resonances on the cross section versus electron energy plot (figure 1(b)) are characteristic of dissociative electron attachment (DEA), a resonant process occurring at low electron energies (<10 eV) characterized by the initial capture of an electron by a molecule to form a transient negative ion that subsequently dissociates into a radical and an anion. In contrast, electron impact excitation and electron impact ionization generally occur at energies above 6 and 10 eV, respectively. The dissociation cross section as a function of electron energy (figure 1(b)) is multiplied by the energy distribution of the secondary electrons (figure 1(a)) to generate the dissociation yield as a function of electron energy (figure 1(c)) for a generic molecule. Even though the dissociation probability increases with increasing incident electron energy, the dissociation yield is thought to be greatest at low incident electron energies (<10 eV) due to the abundance of secondary electrons at those energies (figure 1). However, experimental verification that DEA-initiated processes are dominant in the condensed phase is mostly lacking. Moreover, experimental evidence

[1] Author to whom any correspondence should be addressed.

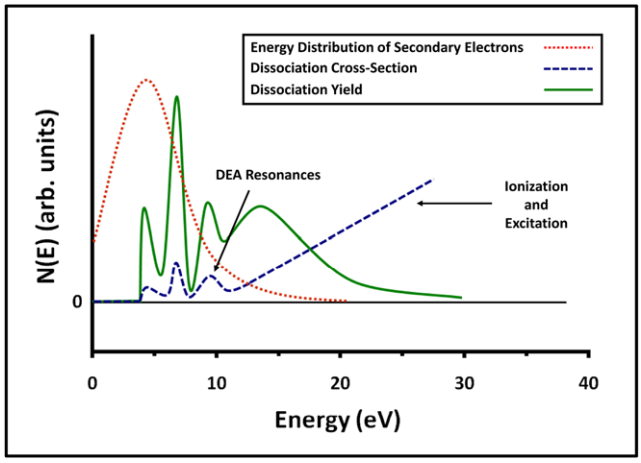

Figure 1. Schematic of (a) energy distribution of secondary electrons generated during a primary ionizing event; (b) cross section for electron-induced dissociation for a typical molecule; (c) dissociation yield as a function of electron energy for a typical molecule. Adapted from a previous publication [2].

suggests that water radiolysis is dominated by ionization followed by electron–ion recombination to yield excited neutral water, which falls apart to H + OH [5]. One goal of the work described herein is to examine the hypothesis that the formation and decay of temporary negative ion resonances by DEA is the dominant mechanism for secondary-electron-induced chemistry associated with high-energy radiolysis.

Dissociative electron attachment to halogenated molecules (RX) to form radicals (·R) and halogen ions (X^-) is a facile process because of the high positive electron affinities of the halogen atoms:

$$e^- + RX \rightarrow RX^- \rightarrow \cdot R + X^-. \tag{1}$$

Because reaction (1) is generally characterized by remarkably high cross sections, especially near 0 eV, DEA is expected to play a prominent role in the high-energy radiolysis of halogenated molecules. As part of a series of post-irradiation studies involving halogenated molecules [6–10], we have chosen to investigate the role of dissociative electron attachment in the condensed phase radiolysis of a simple halocarbon, CF_3I.

The role of dissociative electron attachment in the production of negative ions during electron irradiation of gaseous and condensed phase CF_3I has been investigated [11–13]. Crossed electron/molecular beam experiments were used to identify I^-, CF_3^-, F^- and FI^- as fragment ions of gaseous CF_3I, with I^- producing the strongest anion signal. With a large cross section of 1.4×10^{-14} cm^2, the attachment of a near 0 eV electron to gaseous CF_3I to produce a resonance in the I^- yield at ∼0 eV is an exothermic process, as shown below [11, 14]:

$$\begin{gathered} CF_3I \rightarrow \cdot CF_3 + \cdot I \\ D(CF_3 - I) = 2.39 \pm 0.13 \text{ eV} \end{gathered} \tag{2}$$

$$\begin{gathered} I^- \rightarrow \cdot I + e^- \\ EA(I) = 3.06 \text{ eV} \end{gathered} \tag{3}$$

$$\begin{gathered} CF_3I + e^- \rightarrow \cdot CF_3 + I^- \\ \Delta H_0 = D(CF_3 - I) - EA(I) = -0.67 \text{ eV}. \end{gathered} \tag{4}$$

Dissociative electron attachment to *gaseous* CF_3I to produce F^-, CF_3^- and FI^- occurs via a resonance at 3.8 eV [12]. With a cross section of $\sim 1 \times 10^{-19}$ cm^2, the CF_3^- signal is about five orders of magnitude weaker than the I^- signal at ∼0 eV.

Isothermal electron-stimulated desorption experiments have been used to observe dissociative electron attachment processes during electron-induced reactions of *condensed* CF_3I as well [12]. In contrast to gas phase experiments, CF_3^- is the dominant anion in the condensed phase, with a signal about 200 times stronger than that of I^- [11, 12]. The condensed phase CF_3^- desorption yield resonance peak at ∼4.3 eV can be associated with the structure seen at 3.8 eV in the gas phase experiments. Although gas phase experiments show a clear resonance in the production of F^- at 3.8 eV, desorption of F^- is strongly suppressed below 5 eV in the condensed phase [11, 12]. Instead, the desorption yield of F^- shows two broad, resonance-like structures centered at ∼7 and ∼10 eV. In contrast to the gas phase experiments, the FI^- anion is not observed in the condensed phase [12]. The I^- ion, which produces the strongest anion signal in the gas phase, is detected only in small amounts during condensed phase experiments. Because the desorbed anion must have sufficient kinetic energy to overcome the polarization potential in the condensed phase, some heavy anions such as FI^- and I^-, although formed in significant quantities, might not be detected or detected in small quantities during electron-stimulated desorption studies. Post-dissociation interactions may also diminish the yield of desorbed anions. In addition to a dramatic reduction in signal, the I^- resonance peak shifts from ∼0 eV in the gas phase to ∼2.5 eV in the condensed phase [11, 12]. Although a lower (redshifted) resonance energy may be expected in the condensed phase because of the solvation shift of the anionic potential, interactions with the molecular surroundings may cause a blueshift in the resonance energy if anion desorption is impeded by attractive forces between the anions and the induced charge in the medium. Energy transfer because of post-dissociation interactions may also cause the resonance to shift to a higher energy [11]. It is important to note that the results of our post-irradiation studies of dissociative electron attachment resonances do not suffer from the latter two apparent resonance energy shifts.

The electron-stimulated desorption of CF_3^-, F^- and I^- ions from condensed CF_3I demonstrates the production of ·I, $\cdot CF_2I$ and $\cdot CF_3$ radicals, respectively, by dissociative electron attachment:

$$CF_3I + e^- \rightarrow \cdot I + CF_3^- \tag{5}$$

$$CF_3I + e^- \rightarrow \cdot CF_2I + F^- \tag{6}$$

$$CF_3I + e^- \rightarrow \cdot CF_3 + I^-. \tag{7}$$

The production of FI^- from CF_3I during gas phase experiments [12] suggests the production of $:CF_2$ carbenes by dissociative electron attachment as well:

$$CF_3I + e^- \rightarrow :CF_2 + FI^-. \tag{8}$$

As discussed previously, FI^- likely forms in the condensed phase but does not desorb because of polarization interactions with the surrounding medium.

Whereas previous studies have examined the species (CF_3^-, F^-, I^- and FI^-) desorbing from condensed phase CF_3I at incident electron energies (<15 eV) characteristic of dissociative electron attachment, we have used post-irradiation analysis to investigate the products formed from the complementary species retained in the thin film (·I, ·CF_2I, ·CF_3 and :CF_2). A newly installed low-energy electron gun capable of attaining electron energies as low as 1 eV and a mass spectrometer able to monitor masses above 300 amu have allowed us to identify C_2F_6, C_2F_5I, C_2F_3I, CF_2I_2, $C_2F_4I_2$, CFI_3 and $C_2F_3I_3$ as radiolysis products of condensed CF_3I at an incident electron energy of 4 eV, which is about the threshold for electronic excitation but below the threshold for ionization of CF_3I. Although resonances observed at ∼4 eV in the product yields as functions of electron energy (2–7 eV) suggest the synthesis of these products to occur via dissociative electron attachment, dramatic enhancements in the product yields at 500 eV relative to that at 4 eV for *some* products indicates that DEA is not the dominant mechanism for the high-energy radiation-induced formation of those products. Dissociative electron attachment and/or electron impact excitation, however, may play an important role in high-energy radiation-induced synthesis of the high-yield product C_2F_6.

2. Experimental methods

All post-irradiation temperature-programmed desorption experiments were conducted in a custom-designed stainless steel ultrahigh vacuum (UHV) chamber (base pressure ∼3×10^{-10} Torr) [15]. The chamber is equipped with two quadrupole mass spectrometers, UTI Model 100C and Hiden IDP Series 500, which are capable of detecting masses of up to 300 and 500 amu, respectively. Also attached to the chamber is a low-energy flood electron gun (Kimball Physics model FRA-2X1-2).

The temperature of the Mo(110) single crystal was monitored using a W–5% Re versus W–26% Re thermocouple spot-welded to the crystal. The surface of the crystal was cleaned by first dosing with oxygen at a temperature of 1300 K and then heating briefly to 2200 K. Oxygen reacts with carbon on the crystal surface to form gaseous carbon monoxide, removing any adsorbed carbon contaminants. Excess adsorbed oxygen is then removed when the crystal is heated to 2200 K, which is above the desorption temperature of oxygen.

Gaseous CF_3I (Synquest Labs, lot assay >99% pure) was dosed onto the crystal at 100 K using a direct doser with a precision leak valve (Vacuum Generators MD7). In order to minimize any dose rate effects, the flux of CF_3I molecules incident on the crystal was kept approximately constant. The amount of CF_3I dosed onto the crystal was quantified by using a capacitance manometer (MKS Baratron) to measure the pressure drop in the gas manifold. Temperature-programmed desorption experiments in the absence of electron irradiation were used to determine the coverage of CF_3I, where one monolayer (1 ML) is defined as the coverage achieved by the maximum exposure of the adsorbate that does not yield a multilayer peak.

Irradiation of the CF_3I thin films at 100 K was achieved using a flood electron gun capable of producing energies between 1 and 1000 eV. The spread and zero of the electron energy were determined by measuring the current on the crystal as a function of bias voltage. The energy spread thus measured was less than 0.5 eV at an electron energy of 5 eV. Electron irradiation was followed by radiative heating of the crystal surface to ∼800 K at a rate of ∼10 K s^{-1}. During heating, fragments of species desorbing from the crystal were detected as functions of both time and temperature with one of the two mass spectrometers and a thermocouple interfaced to a computer. No differences in trends were noted between results obtained using the UTI mass spectrometer, which is optimized to detect species desorbing from just the center of the crystal, and the Hiden instrument, which detects species desorbing from the entire surface.

3. Results and discussion

3.1. Identification of electron-induced reaction products

The results of post-irradiation temperature-programmed desorption experiments were used to identify C_2F_6, C_2F_5I, C_2F_3I, CF_2I_2, $C_2F_4I_2$, CFI_3 and $C_2F_3I_3$ as low-energy (4 eV) as well as high-energy (up to 500 eV) electron-induced radiolysis products of condensed CF_3I. Radiolysis products were identified by using a combination of three methods: (1) comparing fragments for desorption features observed in the thermal desorption data to known mass spectra, (2) invoking trends in desorption temperatures and boiling points and (3) comparing results of post-irradiation temperature-programmed desorption experiments to results of γ-radiolysis studies.

Controlled temperature-programmed desorption experiments were conducted by exposing 13 ML of CF_3I at 100 K to photon irradiation but not electron irradiation from the electron gun. Results demonstrate the formation of a small amount of C_2F_6 due to photolysis of CF_3I (figure 2(A)). The results of a post-irradiation temperature-programmed desorption experiment conducted following 4 eV electron irradiation of a 13 ML thin film of condensed CF_3I are shown in figure 2(B). Only the three mass spectral fragments that evinced desorption peaks were monitored in this particular experiment in order to increase the signal-to-noise ratio and to clearly demonstrate the identification of the two radiolysis products C_2F_3I and $C_2F_3I_3$, both of which we failed to identify in our previous work involving 55 eV electron irradiation [16]. Although an extensive search of mass spectral fragments was not performed at incident electron energies above 4 eV, all seven radiolysis products were also observed following high-energy (500 eV) electron irradiation of condensed CF_3I (figure 2(C)). The identification of the 4 eV electron-induced radiolysis products of CF_3I is discussed in detail below.

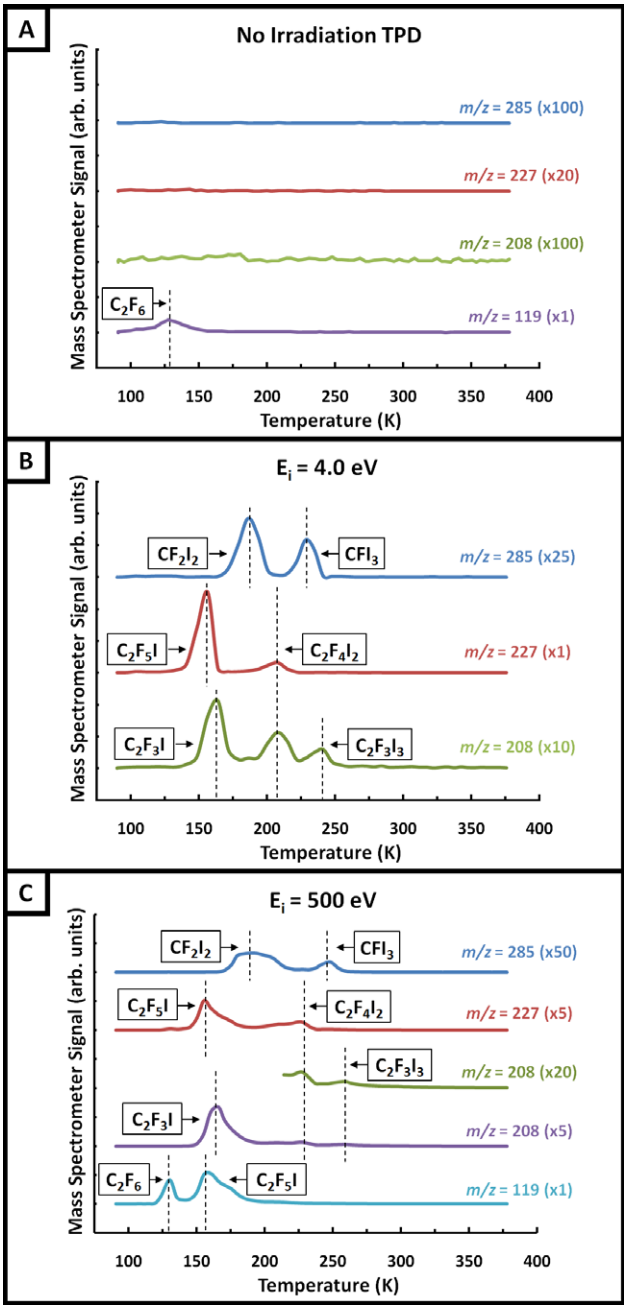

Figure 2. (A) Control temperature-programmed desorption experiment following photon irradiation of a 13 ML CF_3I thin film showing m/z 119 ($C_2F_5^+$), 208 ($C_2F_3I^+$), 227 ($C_2F_4I^+$) and 285 (CFI_2^+). Post-irradiation temperature-programmed desorption data showing the desorption of C_2F_6, C_2F_5I, C_2F_3I, CF_2I_2, $C_2F_4I_2$, CFI_3 and $C_2F_3I_3$ following electron irradiation of 13 ML CF_3I thin films with (B) 4 eV and (C) 500 eV electrons. The total incident electron fluences were 2.7×10^{16} and 1.9×10^{14} electrons cm^{-2}, respectively. The y-axis unit in graphs (B) and (C) are 100 and 16 times larger, respectively, than the corresponding one in (A).

3.1.1. Identification of C_2F_6. Previous γ-radiolysis studies have identified C_2F_6 as a radiolysis product of CF_3I [17, 18]; in addition, C_2F_6 has been reported to desorb from condensed CF_3I on Ni(100) following irradiation with electrons of various energies below 100 eV [19]. The desorption peaks observed at ∼120 K (data not shown) for m/z 100 ($C_2F_4^+$) and 119 ($C_2F_5^+$) were assigned to C_2F_6, as in our previous experiments [16]. The identification of C_2F_6 is supported by the absence of a peak corresponding to the parent m/z 138 ($C_2F_6^+$), which is vanishingly small in the published mass spectrum of C_2F_6 [20].

3.1.2. Identification of C_2F_5I. The desorption features appearing at ∼160 K for fragments m/z 31 (CF^+), 100 ($C_2F_4^+$), 119 ($C_2F_5^+$), 177 (CF_2I^+), 227 ($C_2F_4I^+$) (data shown) and 246 ($C_2F_5I^+$) were assigned to C_2F_5I, in agreement with our previous work [16]. Our identification of C_2F_5I as a radiolysis product of CF_3I is corroborated by C_2F_5I having a higher boiling point (286 K) than C_2F_6 (195 K) [20], consistent with the desorption temperature of C_2F_5I being higher than that of C_2F_6. C_2F_5I has also been previously identified as a γ-radiolysis product of CF_3I [17, 21].

3.1.3. Identification of C_2F_3I. Desorption peaks observed for m/z 189 ($C_2F_2I^+$) (data not shown) and 208 ($C_2F_3I^+$) at ∼165 K were assigned to C_2F_3I. The absence of peaks at m/z 189 and 208 in the C_2F_5I mass spectrum confirms that the species desorbing at ∼165 K is C_2F_3I and not C_2F_5I. Our identification of C_2F_3I is further supported by the absence of desorption peaks at ∼165 K for m/z 258 ($C_3F_5I^+$), 335 ($C_2F_3I_2^+$) and 354 ($C_2F_4I_2^+$), which indicates that the desorbing molecule has fewer than three carbon atoms and fewer than four fluorine atoms. Because C_2F_3I has a higher boiling point (303 K) than C_2F_6 (195 K) [20], our assignment of the desorption peak at ∼165 K to C_2F_3I is consistent with the observed thermal desorption trend for the radiolysis products. Although C_2F_3I was not identified in our previous study, our present results are in agreement with other studies that report the desorption of C_2F_3I following irradiation of condensed CF_3I on Ag(111) and Ni(100) with 100 eV and <110 eV electrons, respectively [19, 22].

3.1.4. Identification of CF_2I_2. The post-irradiation thermal desorption data for CF_3I evinced peaks at ∼185 K for fragments m/z 31 (CF^+), 158 (CFI^+), m/z 254 (I_2^+), 266 (CI_2^+), 285 (CFI_2^+) (data shown) and 304 ($CF_2I_2^+$). These desorption features were attributed to CF_2I_2 based on the presence of a desorption peak for the parent ion, m/z 304 ($CF_2I_2^+$), as well as the absence of desorption peaks in the yields of fragments m/z 208 ($C_2F_3I^+$), 227 ($C_2F_4I^+$), 246 ($C_2F_5I^+$) and 354 ($C_2F_4I_2^+$). Our identification of CF_2I_2 is consistent with data from our previous experiments [16]. Because CF_2I_2 has a higher boiling point (374 K) than C_2F_6 (195 K), C_2F_5I (286 K) and C_2F_3I (303 K) [20], our identification of CF_2I_2 is consistent with the thermal desorption trend for the following four species: C_2F_6 (120 K), C_2F_5I (160 K), C_2F_3I (165 K) and CF_2I_2 (185 K). In addition to being previously identified as a γ-radiolysis product of CF_3I [17, 23, 24], CF_2I_2 has also been identified as an electron-induced radiolysis product of CF_3I at incident electron energies above the ionization threshold [16, 22].

3.1.5. Identification of $C_2F_4I_2$. Desorption peaks observed at ∼210 K for fragments m/z 100 ($C_2F_4^+$), 208 ($C_2F_3I^+$), 227 ($C_2F_4I^+$) (data shown), 254 (I_2^+) and 354 ($C_2F_4I_2^+$) were

assigned to $C_2F_4I_2$, in agreement with our previous work [16]. Because $C_2F_4I_2$ has a higher boiling point (386 K) than CF_2I_2 (374 K) [20], our identification of $C_2F_4I_2$ is consistent with the desorption temperature of $C_2F_4I_2$ being higher than that of CF_2I_2. $C_2F_4I_2$ has been previously identified as a γ-radiolysis product of CF_3I [21].

3.1.6. Identification of CFI_3. A desorption feature for m/z 285 (CFI_2^+) appearing at ~235 K in the post-irradiation thermal desorption data for CF_3I was assigned to the radiolysis product CFI_3. Our identification of CFI_3 is in agreement with our previous data [16], in which desorption features for m/z 139 (CI^+), 158 (CFI^+) and 285 (CFI_2^+) were used to identify CFI_3 as an electron-induced radiolysis product of CF_3I. Because CFI_3 has a boiling point of 477 K [20], our identification of CFI_3 is consistent with the trend in thermal desorption temperatures for the six radiolysis products discussed thus far. CFI_3 formation, however, was not detected following γ-radiolysis [17, 21, 23, 24].

3.1.7. Identification of $C_2F_3I_3$. The post-irradiation thermal desorption data for CF_3I evinced peaks at ~240 K for fragments m/z 208 ($C_2F_3I^+$) and 316 ($C_2F_3I_2^+$) (data not shown) which we attribute to $C_2F_3I_3$. Our identification of $C_2F_3I_3$ as a radiolysis product of CF_3I, a new finding, is corroborated by $C_2F_3I_3$ having a higher boiling point (478 K), higher than CFI_3 (477 K) [20], consistent with the desorption temperature of $C_2F_3I_3$ being higher than that of CFI_3.

3.2. Dynamics of reactions induced by sub-ionization electrons

The dependence of radiolysis product yield on electron energy was investigated by conducting post-irradiation temperature-programmed desorption experiments following irradiation at several different electron energies while maintaining constant electron flux and irradiation time. Film morphology was kept approximately constant by using a constant film deposition rate. Thermal desorption spectra recorded after irradiating 13 ML of CF_3I at incident electron energies of 2.5, 4.0 and 5.5 eV are shown in figure 3. All of the desorption peaks, corresponding to the seven CF_3I radiolysis products, appear to show increases followed by decreases as the incident electron energy is increased.

Additional post-irradiation experiments of 6 ML thick CF_3I films at finer energy intervals between ~1.5 and ~6.5 eV were conducted to further investigate the dependence on incident electron energy. Radiolysis product yields were quantified by integrating the mass spectral peaks for m/z 100 ($C_2F_4^+$), 119 ($C_2F_5^+$), 208 ($C_2F_3I^+$), 227 ($C_2F_4I^+$), 246 ($C_2F_5I^+$), 285 (CFI_2^+), 304 ($CF_2I_2^+$) and 354 ($C_2F_4I_2^+$), which are major mass spectral cracking fragments for radiolysis products C_2F_6, C_2F_5I, C_2F_3I, CF_2I_2, $C_2F_4I_2$ and CFI_3.[2] The radiolysis product yields as functions of electron energy (figure 4) show resonance-like peaks at ~4.0 eV for all of the radiolysis products except C_2F_6. The resonance signatures

[2] The $C_2F_3I_3$ radiolysis product yield was too small to quantify at film thicknesses below 13 ML.

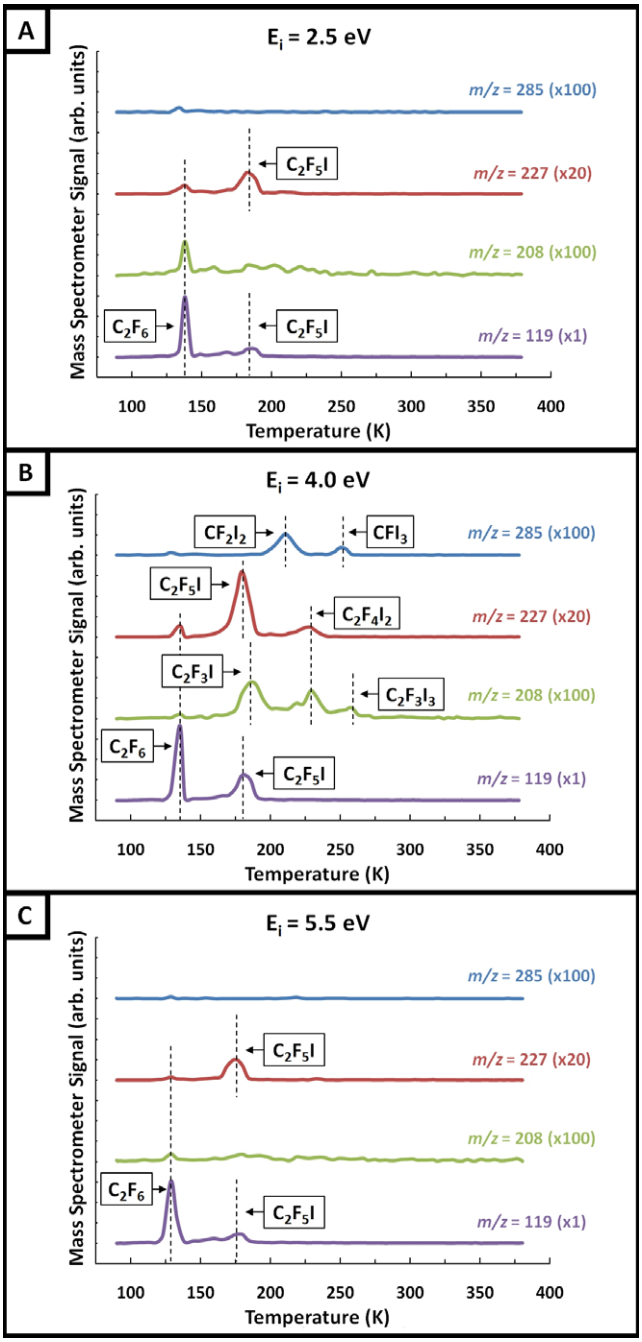

Figure 3. Post-irradiation temperature-programmed desorption data for m/z 119 ($C_2F_5^+$), 208 ($C_2F_3I^+$), 227 ($C_2F_4I^+$) and 285 (CFI_2^+) showing the desorption of C_2F_6, C_2F_5I, C_2F_3I, CF_2I_2, $C_2F_4I_2$, CFI_3 and $C_2F_3I_3$ following electron irradiation of 13 ML thick CF_3I films with (A) 2.5 eV, (B) 4.0 and (C) 5.5 eV electrons. The total incident electron fluence was kept constant at 1.5×10^{16} electrons cm^{-2}.

in the yield functions of these five radiolysis products were clearly observed for all investigated film thicknesses (3, 6 and 9 ML) and electron fluences (3.4×10^{16} and 2.26×10^{16} electrons cm^{-2}). Because the same trends were observed with the UTI mass spectrometer, even though it has a different detection geometry, it is unlikely that the observed resonances are due to experimental artifacts such as variation in electron beam intensity across the crystal surface. The resonances in the

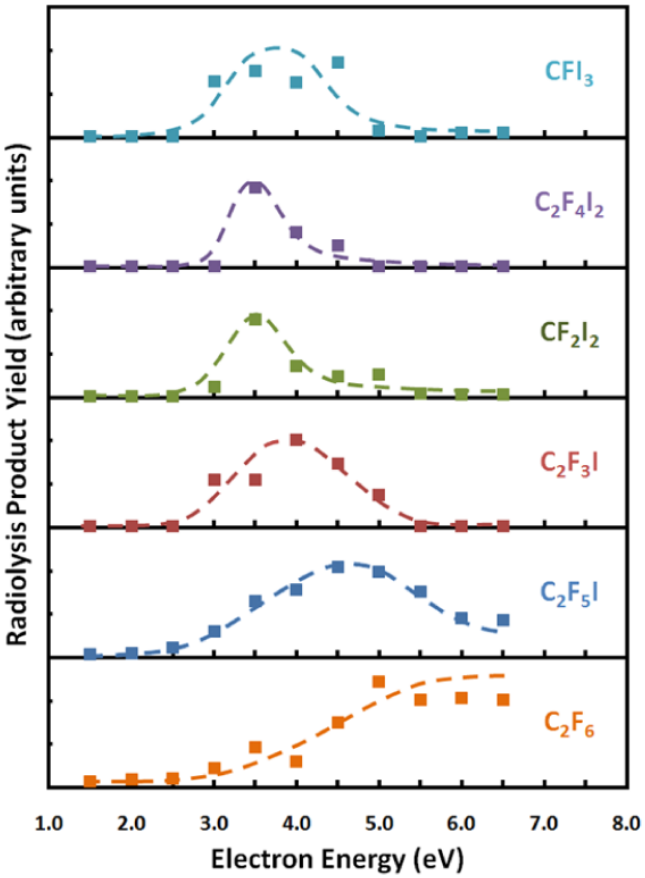

Figure 4. Radiolysis yields for C_2F_6, C_2F_5I, C_2F_3I, CF_2I_2, $C_2F_4I_2$ and CFI_3 plotted as functions of incident electron energy. Film thickness (6 ML) and electron fluence (3.4×10^{16} electrons cm^{-2}) were kept constant.

product yields as functions of incident electron energy indicate that dissociative electron attachment plays a key role in CF_3I radiolysis at sub-ionization incident electron energies.

The formation of the anions CF_3^-, F^- and FI^- from CF_3I at an incident electron energy of ∼4 eV via dissociative electron attachment implies the creation of the complementary species ·I, ·CF_2I and :CF_2, respectively, as described previously (reactions (5), (6) and (8)). Based on an observed resonance in the formation of CFI_3 at ∼4 eV, we suggest that another excited electronic state, which decomposes into F_2^- ions, exists for the temporary negative ion at ∼4 eV:

$$CF_3I + e^- \rightarrow CF_3I^- \rightarrow :CFI + F_2^-. \quad (9)$$

The resulting :CFI carbene can react with CF_3I to form both ·CFI_2 and ·CF_3 radicals:

$$CF_3I + :CFI \rightarrow \cdot CFI_2 + \cdot CF_3. \quad (10)$$

We attribute the non-resonant complex dependence of the C_2F_6 product yield on incident electron energy to multiple pathways for ·CF_3 radical formation involving both resonant dissociative electron attachment and non-resonant electron impact excitation. The formation/desorption at an incident electron energy of ∼0 eV (gas phase)/ ∼2.5 eV (condensed phase) via dissociative electron attachment of the anion I^- from CF_3I implies the creation of the complementary radical ·CF_3, as described previously (reaction (7)). The true location for this resonance in the condensed phase is likely below 4 eV. The second resonant pathway for the formation of the ·CF_3 radicals involving reactions (9) and (10) probably occurs at ∼4 eV. Based on previous photodissociation studies of CF_3I [25, 26], we suggest a third pathway for the formation of ·CF_3 radicals involving electron-induced electronic excitation to a dissociative electronic state of CF_3I followed by prompt dissociation of the C–I bond at incident electron energies above ∼4 eV. Above a threshold of about ∼2.5 eV, the yield of C_2F_6, resulting from the sum of these three mechanisms, appears to increase with incident electron energy more or less monotonically before saturating around 5 eV.

Below we suggest one of several possible reaction mechanisms for each of the seven detected CF_3I radiolysis products formed from four radical (·I, ·CF_2I, ·CFI_2 and ·CF_3) and one carbene (:CF_2) species:

$$\cdot CF_3 + \cdot CF_3 \rightarrow C_2F_6 \quad (11)$$

$$\cdot CF_2I + \cdot CF_3 \rightarrow C_2F_5I \quad (12)$$

$$:CF_2 + \cdot CF_2I \rightarrow C_2F_3I + \cdot F \quad (13)$$

$$\cdot I + \cdot CF_2I \rightarrow CF_2I_2 \quad (14)$$

$$\cdot CF_2I + \cdot CF_2I \rightarrow C_2F_4I_2 \quad (15)$$

$$\cdot I + \cdot CFI_2 \rightarrow CFI_3 \quad (16)$$

$$\cdot CF_2I + \cdot CFI_2 \rightarrow C_2F_3I_3. \quad (17)$$

A more complete list of possible reaction mechanisms may be found elsewhere [16, 22].

3.3. Radiolysis by high-energy electrons

As discussed previously, all seven CF_3I electron-induced reaction products were also identified following irradiation with 500 eV electrons. Other non-resonant mechanisms besides dissociative electronic excitations that yield neutral fragments become available at such high incident electron energies. For example, dissociative ionization of CF_3I to yield CF_3^+ and CF^+ occurs above a threshold of about 12 and 22 eV, respectively [27]. Electron impact excitation of CF_3I followed by non-resonant ion pair formation (dipolar dissociation) above a threshold of about 12 eV yields F^-, CF_2I^+, CF_3^- and I^+ [12, 13]. Nevertheless, the commonality in electron-induced reaction products is suggestive of a similarity in reaction intermediates and mechanisms at both low and high incident electron energies.

The yields per incident electron at low and high incident electron energies for each electron-induced reaction product were compared to ascertain the role of sub-ionization electrons in the high-energy radiolysis of condensed CF_3I (table 1). We estimate that the measured relative yield values are accurate to within one order of magnitude. At first glance, the dependence of the radiolysis product yield on incident electron energy (4–500 eV) is consistent with a superposition of multiple non-resonant excitation and ionization events,

Table 1. The relative yields per incident electron at 4, 15, 55 and 500 eV electron energies for each of the seven electron-induced reaction products. The yields have been normalized to the corresponding values at 4 eV. Yields were calculated from post-irradiation temperature-programmed desorption experiments conducted following electron irradiation of 13 ML thick CF_3I films. Although the incident electron flux was kept constant for all of the experiments, the irradiation time was varied between 1200 s (4 eV) and 30 s (500 eV).

	4 eV	15 eV	55 eV	500 eV
C_2F_6	1	1×10^1	2×10^2	4×10^2
C_2F_5I	1	1×10^1	2×10^2	1×10^3
C_2F_3I	1	1×10^0	7×10^2	2×10^4
CF_2I_2	1	1×10^1	7×10^2	3×10^3
$C_2F_4I_2$	1	1×10^1	3×10^2	6×10^3
CFI_3	1	2×10^1	2×10^3	6×10^3
$C_2F_3I_3$	1	2×10^1	7×10^2	4×10^3

each of which is characterized by a monotonically rising signal above a thermodynamic threshold. Nevertheless, the secondary electrons produced at incident electron energies above 15 eV must also contribute to the radiolysis yield because such electrons, depending on the kinetic energy with which they are created, may dissociate molecules via ionization, excitation and dissociative electron attachment. Secondary electrons from the metal substrate should be negligible because of the relatively thick 13 ML films used in these experiments. Although we do not have a method to quantify the secondary electron distribution in condensed CF_3I, our results indicate that low-yield radiolysis products such as CFI_3 have enhancement factors that are too large to be explained by sub-ionization secondary-electron-induced reaction mechanisms alone. Relatively low enhancement factors for the high-yield radiolysis product C_2F_6, however, indicates that dissociative electron attachment and/or electron impact excitation induced by secondary electrons may be the dominant mechanism for the high-energy radiation-induced synthesis in condensed CF_3I. It is also important to note that, because of the very strong resonance at 0 eV for the formation of $\cdot CF_3$ radicals from CF_3I, C_2F_6 may be formed in copious amounts at electron energies below 1 eV, an energy regime not easily accessed with electron guns.

4. Conclusions

Results of post-irradiation temperature-programmed desorption experiments were used to identify C_2F_6, C_2F_5I, C_2F_3I, CF_2I_2, $C_2F_4I_2$, CFI_3 and $C_2F_3I_3$ as low-energy (4 eV) electron-induced products of condensed CF_3I. At this sub-ionization incident electron energy, the dominant mechanism for C_2F_6 formation appears to be electron impact excitation, whereas dissociative electron attachment plays a critical role in the synthesis of the other six products. Our results indicate that dissociative electron attachment and/or electron impact excitation may play an important role in high-energy radiation-induced synthesis of the high-yield product C_2F_6. For the formation of products such as CFI_3, however, dissociative electron attachment appears not to play a dominant role. To ascertain whether the formation and decay of temporary negative ion resonances is the dominant mechanism for secondary electron-induced damage associated with radiolysis, one must conduct similar post-irradiation experiments that measure the relative yields, at low and high incident electron energy, of many different target molecules including those with lower propensity for dissociative electron attachment.

Acknowledgments

This work was supported by grants from the National Science Foundation (NSF grant nos. CHE-0455278 and CHE-0353813). CRA gratefully acknowledges the late Professor Ted Madey for his inspirational mentorship.

References

[1] Kaplan I G and Miterev A M 1987 *Adv. Chem. Phys.* **68** 255
[2] Mason N J 2003 *AIP Conf. Proc.* **680** 885
[3] Bass A D and Sanche L 2004 Interactions of low-energy electrons with atomic and molecular solids *Charged Particles and Photon Interactions with Matter* ed A Mozumder and Y Hatano (New York: Dekkar) p 207
[4] Arumainayagam C R, Lee H D, Nelson R B, Haines D R and Gunawardane R 2010 *Surf. Sci. Rep.* **65** 144
[5] Kimmel G A and Orlando T M 1995 *Phys. Rev. Lett.* **75** 2606
[6] Nakayama N, Wilson S C, Stadelmann L E, Lee H-L D, Cable C A and Arumainayagam C R 2004 *J. Phys. Chem.* B **108** 7950
[7] Nakayama N, Ferrenz E E, Ostling D R, Nichols A S, Faulk J F and Arumainayagam C R 2004 *J. Phys. Chem.* B **108** 4080
[8] Bass A D, Arumainayagam C R and Sanche L 2008 *Int. J. Mass Spectrom.* **277** 251
[9] Weeks L D, Zhu L L, Pellon M, Haines D R and Arumainayagam C R 2007 *J. Phys. Chem.* C **111** 4815
[10] Rajappan M, Zhu L L, Bass A D, Sanche L and Arumainayagam C R 2008 *J. Phys. Chem.* C **112** 17319
[11] Le Coat Y, Azria R, Tronc M, Ingolfsson O and Illenberger E 1998 *Chem. Phys. Lett.* **296** 208
[12] Oster T, Ingolfsson O, Meinke M, Jaffke T and Illenberger E 1993 *J. Chem. Phys.* **99** 5141
[13] Heni M and Illenberger E 1986 *Chem. Phys. Lett.* **131** 314
[14] Underwood-Lemons T, Gergel T J and Moore J H 1995 *J. Chem. Phys.* **102** 119
[15] Harris T D, Lee D H, Blumberg M Q and Arumainayagam C R 1995 *J. Phys. Chem.* **99** 9530
[16] Nakayama N, Ferrenz E E, Ostling D R, Nichols A S, Faulk J F and Arumainayagam C R 2004 *J. Phys. Chem.* B **108** 4080
[17] Hsieh T and Hanrahan R J 1978 *Radiat. Phys. Chem.* **12** 153
[18] Shah P G, Stranks D R and Cooper R 1970 *Aust. J. Chem.* **23** 253
[19] Jensen M B and Thiel P A 1995 *J. Am. Chem. Soc.* **117** 438
[20] NIST Chemistry WebBook 2005 *NIST Standard Reference Database Number 69* National Institute of Standards and Technology, June
[21] Teclemariam D and Hanrahan R J 1982 *Radiat. Phys. Chem.* **19** 443
[22] Fieberg J E, Szabo A and White J M 1996 *J. Chem. Soc. Faraday Trans.* **92** 4739
[23] McAlpine I and Sutcliffe H 1969 *J. Phys. Chem.* **73** 3215
[24] McAlpine I and Sutcliffe H 1970 *J. Phys. Chem.* **74** 1422
[25] Rattigan O V, Shallcross D E and Cox R A 1997 *J. Chem. Soc. Faraday Trans.* **93** 2839
[26] Aguirre F and Pratt S T 2003 *J. Chem. Phys.* **119** 9476
[27] Christophorou L G and Olthoff J K 2000 *J. Phys. Chem. Ref. Data* **29** 553